JACS
JOURNAL OF THE AMERICAN CHEMICAL SOCIETY

Subscriber access provided by American Chemical Society

Article

Mechanisms of Water Oxidation Catalyzed by the *cis*,*cis*-[(bpy)Ru(OH)]O Ion

Hiroshi Yamada, William F. Siems, Tohru Koike, and James K. Hurst

J. Am. Chem. Soc., **2004**, 126 (31), 9786-9795• DOI: 10.1021/ja030594g • Publication Date (Web): 14 July 2004

Downloaded from http://pubs.acs.org on April 1, 2009

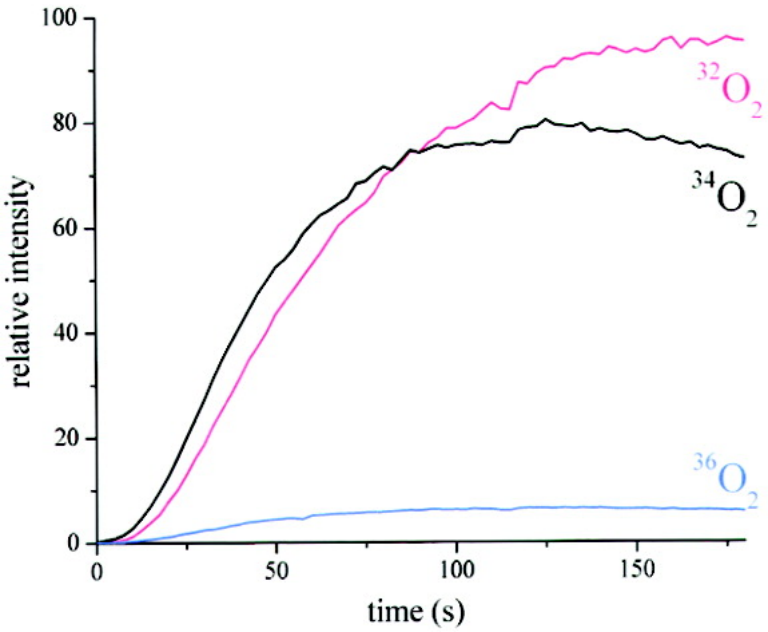

More About This Article

Additional resources and features associated with this article are available within the HTML version:

- Supporting Information
- Links to the 13 articles that cite this article, as of the time of this article download
- Access to high resolution figures
- Links to articles and content related to this article
- Copyright permission to reproduce figures and/or text from this article

View the Full Text HTML

ACS Publications
High quality. High impact.

Journal of the American Chemical Society is published by the American Chemical Society. 1155 Sixteenth Street N.W., Washington, DC 20036

J|A|C|S
ARTICLES
Published on Web 07/14/2004

Mechanisms of Water Oxidation Catalyzed by the *cis,cis*-$[(bpy)_2Ru(OH_2)]_2O^{4+}$ Ion

Hiroshi Yamada,[†] William F. Siems,[‡] Tohru Koike,[†] and James K. Hurst*,[‡]

Contribution from the Department of Chemistry, National Defense Academy, 1-10-20 Hashirimizu, Yokosuka, Kanagawa 239, Japan, and Department of Chemistry, Washington State University, Pullman, Washington 99164-4630

Received October 23, 2003; Revised Manuscript Received May 10, 2004; E-mail: hurst@wsu.edu

Abstract: The *cis,cis*-$[(bpy)_2Ru^{III}(OH_2)]_2O^{4+}$ μ-oxo dimeric coordination complex is an efficient catalyst for water oxidation by strong oxidants that proceeds via intermediary formation of *cis,cis*-$[(bpy)_2Ru^{V}(O)]_2O^{4+}$ (hereafter, {5,5}). Repetitive mass spectrometric measurement of the isotopic distribution of O_2 formed in reactions catalyzed by ^{18}O-labeled catalyst established the existence of two reaction pathways characterized by products containing either one atom each from a ruthenyl O and solvent H_2O or both O atoms from solvent molecules. The apparent activation parameters for μ-oxo ion-catalyzed water oxidation by Ce^{4+} and for {5,5} decay were nearly identical, with $\Delta H^{\ddagger} = 7.6$ ($\pm$1.2) kcal/mol, $\Delta S^{\ddagger} = -43$ ($\pm$4) cal/deg mol (23 °C) and $\Delta H^{\ddagger} = 7.9$ ($\pm$1.1) kcal/mol, $\Delta S^{\ddagger} = -44$ ($\pm$4) cal/deg mol, respectively, in 0.5 M CF_3SO_3H. An apparent solvent deuterium kinetic isotope effect (KIE) of 1.7 was measured for O_2 evolution at 23 °C; the corresponding KIE for {5,5} decay was 1.6. The $^{32}O_2/^{34}O_2$ isotope distribution was also insensitive to solvent deuteration. On the basis of these results and previously established chemical properties of this class of compounds, mechanisms are proposed that feature as critical reaction steps H_2O addition to the complex to form covalent hydrates. For the first pathway, the elements of H_2O are added as OH and H to the adjacent terminal ruthenyl O atoms, and for the second pathway, OH is added to a bipyridine ring and H is added to one of the ruthenyl O atoms.

Introduction

Almost 20 years ago, T. J. Meyer's group reported that *cis,cis*-$[(bpy)_2Ru(OH_2)]_2O^{4+}$ was a remarkably effective catalyst for water oxidation by strong oxidants.[1] This report stimulated considerable global interest in the underlying chemical reaction mechanisms, which have been viewed as relevant to biological reactions involving metal dinuclear and tetranuclear μ-oxo reaction centers[2] and potentially important to development of practical devices for large-scale energy utilization.[3] However, despite subsequent intensive investigation of reactions catalyzed by this ion and related complexes of the general formula *cis,cis*-$[L_2Ru(OH_2)]_2O^{n+}$,[4-6] the reaction mechanisms remain obscure. (In the general formula, L represents a functionalized congener of 2,2′-bipyridine or a related diimine.)

Scheme 1. Detectable Redox States of the μ-Oxo Ion[8a]

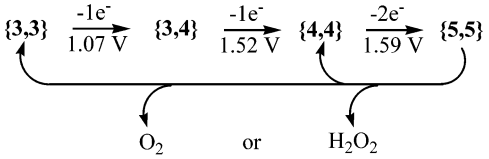

[a] The reduction potentials shown are for 0.5 M CF_3SO_3H and are referenced against NHE.[7] Decay of {5,5} may lead to either H_2O_2 or O_2 as the immediate product.

In earlier redox titrimetric and electrochemical studies, we established that, in dilute trifluoromethanesulfonic (triflic) acid, the $[(bpy)_2Ru(OH_2)]_2O^{4+}$ ion undergoes progressive one- and two-electron oxidations with equivalent loss of protons to give ultimately the corresponding 4 e^--oxidized product (designated {5,5} in Scheme 1) containing ruthenyl oxo atoms in place of the original water molecules.[7] As discussed herein, the {5,5} ion undergoes first-order decay to the {4,4} ion with rate parameters that approximate those for O_2 formation measured under steady-state conditions,[9] indicating that the {5,5} ion is either the O_2-evolving species or its immediate precursor. In contrast, decay of the lower oxidation states (Scheme 1) is too slow for them to be directly involved in O_2 formation. A variety of mechanisms have been proposed for this reaction that focus almost universally upon the ruthenyl group. As summarized in

[†] National Defense Academy.
[‡] Washington State University.

(1) Gilbert, J. A.; Eggleston, D. S.; Murphy, W. S., Jr.; Geselowitz, D. A.; Gersten, S. W.; Hodgson, D. J.; Meyer, T. J. *J. Am. Chem. Soc.* **1985**, *107*, 3855−3864.
(2) See, for example: (a) Hoganson, C. W.; Babcock, G. T. *Science* **1997**, *277*, 1953−1956. (b) Pecoraro, V. L.; Baldwin, M. J.; Caudle, M. T.; Hsieh, W.-Y.; Law, N. A. *Pure Appl. Chem.* **1998**, *70*, 925−929.
(3) (a) *Energy Resources through Photochemistry and Catalysis*; Grätzel, M. Ed.; Academic Press: New York, 1983. (b) *Photochemical Conversion and Storage of Solar Energy*; Connolly, J. S., Ed.; Academic Press: New York, 1981.
(4) Extensive compilations of earlier papers are given in refs 5 and 6.
(5) Chronister, C. W.; Binstead, R. A.; Ni, J.; Meyer, T. J. *Inorg. Chem.* **1997**, *36*, 3814−3815.
(6) Lei, Y.; Hurst, J. K. *Inorg. Chem.* **1994**, *33*, 4460−4467.
(7) Yamada, H.; Hurst, J. K. *J. Am. Chem. Soc.* **2000**, *122*, 5303−5311.

10.1021/ja030594g CCC: $27.50 **© 2004 American Chemical Society**

Scheme 2. Representative Pathways for O−O Bond Formation Involving the Diruthenyl Unit of the {5,5} Ion[a]

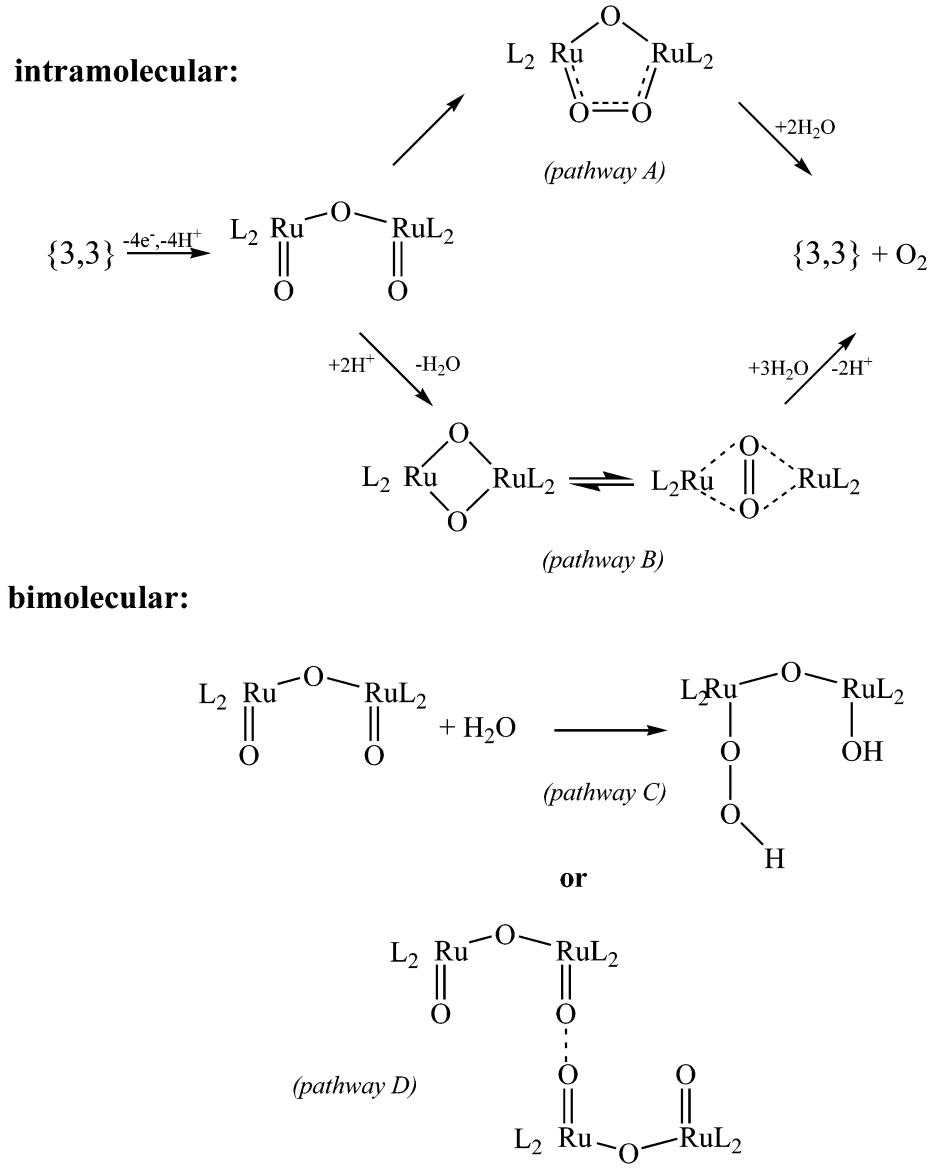

[a] Only key intermediates are shown.

Scheme 2, they include reductive elimination of ruthenyl oxo atoms derived from coordinated aqua ligands in higher oxidation states of the μ-oxo ion, forming either O_2 directly or H_2O_2 as a reaction intermediate;[10,11] analogous bimolecular reactions involving two catalyst ions;[12] and reactions between solvent H_2O and ruthenyl oxo atoms, leading to incorporation of either one or two solvent oxygen atoms in the final O_2 product.[12−14]

In the present study, we describe mass spectrometric methods that allow one to follow in real time the course of evolution of O_2 in the {5,5} ion. Using ^{18}O-isotopically enriched catalyst, we show that the isotopic distribution of O_2 obtained is quantitatively accountable by invoking two reaction pathways, both of which involve incorporation of solvent oxygen atoms in the reaction product. These studies eliminate from further consideration pathways that involve either (1) internal rearrangement within a single complex ion with reductive elimination of O_2 or (2) bimolecular reactions between two complex ions with direct O−O bond formation between their coordinated oxygen-containing ligands. Furthermore, the measured temperature and deuterium solvent isotope dependencies of O_2 evolution rates appear inconsistent with a simple bimolecular reaction between H_2O and the {5,5} ion, but rather

(8) The electrons involved in forming the μ-oxo bridge are extensively delocalized over the Ru−O−Ru unit (see, for example: Weaver, T. R.; Meyer, T. J.; Adeyemi, S. A.; Brown, G. M.; Eckberg, R. P.; Hatfield, W. E.; Johnson, E. C.; Murray, R. W.; Untereker, D. *J. Am. Chem. Soc.* **1975**, *97*, 3039−3048). Thus, for example, the notation {3,4} signifies that the Ru−O−Ru unit contains 13 π-symmetry electrons (with four originating in O^{2-}), but is not meant to imply the existence of discrete valence-localized ruthenium d^4 and d^5 ions.

(9) Lei, Y.; Hurst, J. K. *Inorg. Chim. Acta* **1994**, *226*, 179−185.

(10) Rotzinger, F. P.; Munavalli, S.; Comte, P.; Hurst, J. K.; Grätzel, M.; Frank, A. J. *J. Am. Chem. Soc.* **1987**, *109*, 6619−6626.

(11) Comte, P.; Nazeruddin, F. P.; Rotzinger, F. P.; Frank, A. J.; Grätzel, M. *J. Mol. Catal.* **1989**, *52*, 63−84.

(12) Binstead, R. A.; Chronister, C. W.; Ni, J.; Hartshorn, C. M.; Meyer, T. J. *J. Am. Chem. Soc.* **2000**, *122*, 8464−8473.

(13) Hurst, J. K.; Zhou, J.; Lei, Y. *Inorg. Chem.* **1992**, *31*, 1010−1017.

(14) Meyer, T. J. In *Oxygen Complexes and Oxygen Activation by Transition Metals*; Martell, A. E.; Sawyer, D. T., Eds.; Plenum Press: New York, 1988; pp 33−48.

suggest that O_2 formation is preceded by rate-limiting unimolecular activation of the complex ion, perhaps by internal electronic rearrangement. A novel reaction mechanism is proposed that features formation of a bipyridyl ligand π-cation with reaction of solvent at that site; this mechanism may have precedents in water oxidation and other ligand reactions reported for a broader range of ruthenium bipyridyl complexes.[15−22]

Experimental Section

Materials. The μ-oxo-bridged dimeric ruthenium coordination complex *cis,cis*-$[(bpy)_2Ru(OH_2)]_2O^{4+}$ was prepared as the perchlorate salt following well-established synthetic procedures[1] and was recrystallized repeatedly to remove minor impurities.[7] The final product was isolated as fine dark blue crystalline needles that were ~1 mm in length. Concentrations of reagent solutions of the {3,3} ion were determined spectrophotometrically using $\epsilon_{636} = 2.2 \times 10^4\ M^{-1}\ cm^{-1}$.[7] Purity was established by spectroscopically monitoring one-electron oxidative titrations of the {3,3} ion in 0.5−1.0 M trifluoromethanesulfonic (triflic) acid with Ce^{4+}. These reactions occurred with $[Ce^{4+}]/[\{3,3\}]$ stoichiometries of 1.0. Five sharp isosbestic points (at 533, 404, 340, 294, and 261 nm) were observed in the optical spectra over the course of the titration, and changes in the absorption maxima of {3,3} at 636 nm and {3,4} at 448 nm were proportional to the amount of added Ce^{4+}. The visible isosbestic points are particularly good criteria of purity because the impurities formed during preparation absorb strongly in these regions. Reagent solutions of the complex containing ^{18}O-isotopically enriched aqua ligands were prepared by incubating the {3,3} ion (typically, at 7.5 mM) in 97.2% $[^{18}O]$-H_2O (ICON) to which had been added sufficient triflic anhydride to give 0.5 M triflic acid. After ~90 min at room temperature, the complex was oxidatively titrated to the {3,4} state with a slight stoichiometric excess (~5%) of concentrated Ce^{4+}. Under these conditions, the reaction half-times for water exchange at the *cis*-aqua position were $t_{1/2} \approx 2$ min for the {3,3} ion and $t_{1/2} >$ 80 d for the {3,4} ion;[18] exchange of the bridging μ-oxo atom with solvent H_2O did not occur in either oxidation state.[7,13] The ^{18}O-isotopically enriched {3,4} ions were kept in $H_2{}^{18}O$ until immediately before their use in isotope tracer experiments, which was always within a few hours of their preparation. The final enrichments were calculated by assuming that the ^{16}O atoms introduced upon addition of triflic anhydride equilibrated with solvent $H_2{}^{16}O$ during the incubation period and that the isotopic composition at the *cis*-aqua positions were identical to the final solvent composition. As calculated, the enrichments for these preparations were 89−91%. Solutions of the analogous complex containing ^{18}O in the bridging position, that is, $[(bpy)_2Ru(^{18}OH_2)]_2{}^{18}O^{4+}$, were prepared from *cis*-$Ru(bpy)_2Cl_2$ in ^{18}O-enriched H_2O using the same procedures as normal {3,3} ion.[13] In this case, however, the limited availability of $H_2{}^{18}O$ precluded purification of the product. Triflic acid (99% CF_3SO_3H, Alfa Aesar) was vacuum-distilled and stored at 10 °C as 0.5−1.0 M aqueous solutions. Other chemicals were reagent grade and used as received from commercial suppliers; water was purified using a Milli-Q ion exchange/reverse osmosis system.

Analytical Methods. The kinetics of decay of the {5,5} ion were monitored spectrophotometrically by using a computer-interfaced HP 8452A diode array instrument. For most experiments, the {5,5} ion was prepared electrochemically by using a carbon fiber columnar flow electrolysis cell attached to a potentiostat as previously described.[7] To conserve the dimeric coordination complex, the electrolysis cell was modified for experiments measuring the temperature dependence of {5,5} decay. In this case, a thin 5.9 mm i.d. porous Vycor tube (Bioanalytical Systems) filled with carbon fibers was used in place of the larger standard 8.2 mm i.d. electrode, allowing preparation of the {5,5} ion at a slower flow rate. The effluent from the cell was run directly into a 1 mm or 2 mm optical cell and the UV−vis spectra were repetitively recorded following stoppage of the flow. Oxygen evolution experiments were conducted using reaction chambers composed of 6−10 mL reservoirs encased within outer glass chambers through which thermostated fluids could be circulated from a constant-temperature bath. Access to the reaction chamber was provided by two 2 mm bore capillary glass tubes through which purging gases or reagents could be introduced and a larger ~12 mm tube whose diameter was appropriate to receive a YSI model 5331 oxygen probe. This probe was fitted with O-rings to achieve an airtight seal within the tube. Rates of O_2 evolution were made on continuously stirred argon-purged samples with the probe located within the gaseous headspace region of the reaction chamber. In a typical run, reaction was initiated by syringe addition of 0.25 mL of 0.30 M Ce^{4+} through a septum to 6.75 mL of acidic solutions containing 0.10 mM of the {3,3} ion, and the response of the electrode was recorded as a function of time using a strip-chart recorder. The electrode was calibrated by measuring the amplitude of the pen deflection when air originally present in the chamber was replaced by Ar. For experiments measuring the mass distributions of gases formed in the reaction chamber, the O_2 electrode was replaced by a Lucite plug in which was mounted one end of a glass capillary column. In a typical run, 0.9 mL of 0.25 M Ce^{4+} was added to 8.1 mL of 0.5 M triflic acid containing 0.04−0.8 mM of the ^{18}O-isotopically enriched complex ion prepared as described in the preceding section. Headspace gases were continuously withdrawn at ~1 mL/min into a VG7070EHF double-focusing mass spectrometer operated in the EI mode at 70 eV with a 10−50 *m*/*z* continuum scan. The purging gas used in these experiments was He. A 10 mL syringe containing He was attached via a Hamilton three-way valve to one of the sidearms of the reaction cell. During runs, the valve was opened to the reaction chamber, allowing gases withdrawn by the mass spectrometer to be replaced by He, thereby maintaining normal atmospheric pressure in the chamber. Ceric ion was introduced via syringe transfer through the other sidearm of the reaction cell to initiate the reaction. Resonance Raman (RR) spectra were acquired at room temperature by using 90° scattered light from sealed samples in glass capillaries. The Raman spectrometer, which uses a McPherson 2061 spectrograph coupled to a Princeton Instruments LN-1100PB CCD detector, has been previously described.[23,24]

Data Analyses. To avoid complications associated with the slow secondary conversion of {4,4} to {3,4}, decay of the {5,5} ion was analyzed from changes in optical absorption at wavelengths corresponding to the isosbestic points of the {4,4} and {3,4} ions (470 nm in 0.5 M triflic acid/H_2O and 468 nm in 0.5 M triflic acid/D_2O). At these wavelengths, the reactions exhibited simple first-order behavior over 3 to 4 half-lives. Determination of O_2 evolution rates required knowledge of the headspace volume in the reaction cell, which was estimated from the difference in weight of the cell when empty and filled with H_2O. Variations in the effective volume for a given run were estimated to introduce a 10−15% uncertainty in the O_2 rates, which were calculated in units of nmol O_2 formed/s. Prior studies had established that these rates were linearly dependent upon $[\{5,5\}]$.[7,9] The turnover number (k_{cat}), which is a first-order rate constant, was determined by dividing the O_2 formation rate by the amount of catalyst present in the cell.

(15) Creutz, C.; Sutin, N. *Proc. Natl. Acad. Sci. U.S.A.* **1975**, *72*, 2858−2862.
(16) Nord, G.; Pedersen, B.; Bjergbakke, E. *J. Am. Chem. Soc.* **1983**, *105*, 1913−1919.
(17) Ghosh, P. K.; Brunschwig, B. S.; Chou, M.; Creutz, C.; Sutin, N. *J. Am. Chem. Soc.* **1984**, *106*, 4772−4783.
(18) Ledney, M.; Dutta, P. K. *J. Am. Chem. Soc.* **1995**, *117*, 7687−7695.
(19) Berg-Brennan, C.; Subramanian, P.; Absi, M.; Stern, C.; Hupp, J. T. *Inorg. Chem.* **1996**, *35*, 3719−3722.
(20) Zhang, H.-T.; Yan, S. G.; Subramanian, P.; Skeens-Jones, L. M.; Stern, C.; Hupp, J. T. *J. Electroanal. Chem.* **1996**, *414*, 23−29.
(21) Rollick, K. L.; Kochi, J. K. *J. Org. Chem.* **1982**, *47*, 435−444.
(22) Sagüés, J. A. A.; Gillard, R. D.; Lancashire, R. J.; Williams, P. A. *J. Chem. Soc., Dalton Trans.* **1979**, 193−198.
(23) Yamada, H.; Koike, T.; Hurst, J. K. *J. Am. Chem. Soc.* **2001**, *123*, 12775−12780.
(24) Nakamura, N.; Moënne-Loccoz, P.; Tanizawa, K.; Mure, M.; Suzuki, S.; Klinman, J. P.; Sanders-Loehr, J. *Biochemistry* **1997**, *36*, 11479−11486.

Isotopic distributions of $^{32}O_2$, $^{34}O_2$, and $^{36}O_2$ formed in the catalyzed reaction were corrected for background counts by subtracting the averaged intensities at these masses for 10−20 scans immediately prior to adding Ce^{4+}. Typically, these corrections to the data amounted to <10% for $^{34}O_2$, but were 30−80% for the other ions, with the relative magnitude of the background correction decreasing progressively as the reaction proceeded and O_2 accumulated in the reaction cell. The reasons for the relative large corrections for $^{32}O_2$ and $^{36}O_2$ differed, however. The background intensity for $^{32}O_2$ was relatively large because of the presence of air in the spectrometer, whereas the amount of $^{36}O_2$ produced in the catalyzed reaction was exceedingly small and did not rise appreciably above the low background intensities recorded at this mass. The relative yields of the three isotopes in individual scans were calculated from the background-corrected mass intensities; as described in the Results section, plots of these data vs time were made and extrapolated to $t = 0$ to obtain the isotope distribution from the catalyzed reaction at the start of the reaction. This procedure corrects for the small amount of isotopic dilution that occurs by incorporation of coordinated ^{34}O into the O_2 product and its subsequent replacement in the Ru coordination sphere by ^{32}O from the solvent. The refined data were analyzed by recognizing that there exist three possible types of reaction pathways, defined by whether the O_2 formed contains zero, one, or two O atoms obtained from the coordinated ruthenyl O atoms. From the estimated isotopic composition of the ^{18}O-enriched $[(bpy)_2Ru(O)]_2O^{4+}$ ions used in the reaction and the known composition of the reaction solution, one can calculate the O_2 isotopic distribution expected for each of these types of pathways. These distributions can then be used with the experimentally determined yields of $^{32}O_2$, $^{34}O_2$, and $^{36}O_2$ to evaluate the relative contributions of each of the pathways in the overall reaction. In practice, this evaluation made use of the following equations:

$$\%\ (^{32}O_2)\ \text{formed} = a_1x + b_1y + c_1z$$

$$\%\ (^{34}O_2)\ \text{formed} = a_2x + b_2y + c_2z$$

where x, y, and z represent the fractional contributions of each of the pathways, a_1 and a_2 are the percent formation of $^{32}O_2$ and $^{34}O_2$ predicted for pathway x under the prevailing conditions, and the pairs b_1,b_2 and c_1,c_2 are analogously defined for pathways y and z. Simultaneous solution of these equations subject to the constraint, $x + y + z = 1$, gives unique values for x, y, and z.

Results

^{18}O-Isotopic Labeling Studies. Use of closed reaction cells configured as described in the Experimental Section allowed rapid repetitive determination of the mass distributions of gaseous products evolved from triflic acid solutions containing the catalyst and the strong oxidizing Ce^{4+} ion. In these experiments, $[(bpy)_2Ru(OH_2)]_2O^{4+}$ ions that were isotopically enriched in their *cis*-aqua positions were first oxidized to their {3,4} oxidation state while in ^{18}O-enriched H_2O to minimize any subsequent water exchange upon addition to isotopically dilute solvent.[23] Then, following brief bubbling with He to remove air, the reaction was initiated by syringe-addition of excess Ce^{4+}, causing near-quantitative oxidation of the catalyst to its {5,5} oxidation state. Throughout this procedure and during the initial stages of the reaction, headspace gases were scanned every 2.0 to 2.5 s over the range of 10−50 amu. The recorded intensities at 32, 34, and 36 amu of a typical run are displayed in Figure 1a. Prior to addition of the oxidant, intensities at 34 and 36 amu levels are negligible. The intensity at 32 amu is measurable, but unchanging; it represents the background level of O_2 in the instrument. Upon addition of Ce^{4+},

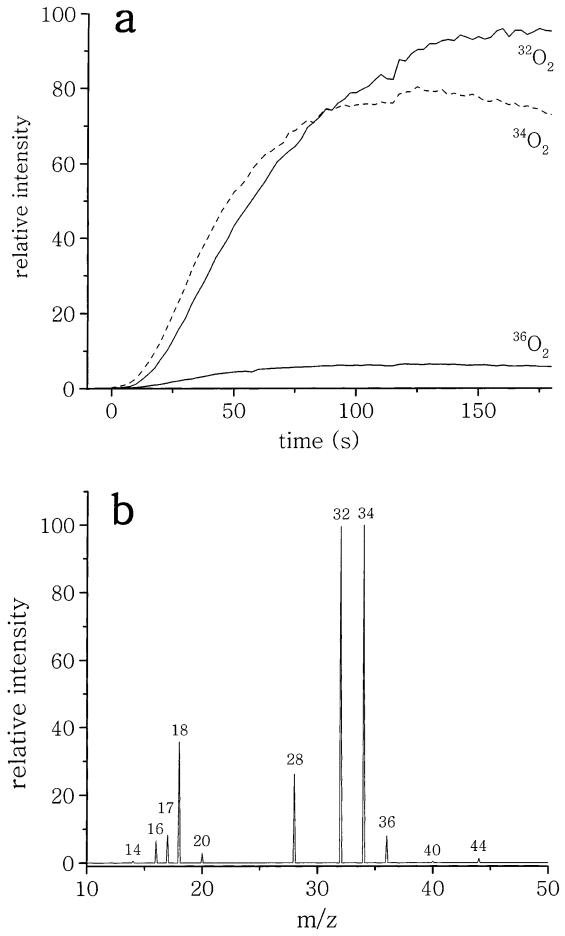

Figure 1. Mass spectrometric analysis of evolved gases from μ-oxo ion-catalyzed water oxidation. (a) Changes in peak intensities of O_2 isotopes at ambient temperature following addition of Ce^{4+} to give a final solution composition of 0.86 mM 89.4% ^{18}O-enriched *cis*,*cis*-$[(bpy)_2Ru(^{18}O)]_2O^{4+}$ plus 25 mM Ce^{4+} in 7.8% ^{18}O-enriched H_2O (0.5 M CF_3SO_3H). As indicated, the upper and lower solid lines refer to intensities at 32 and 36 amu, and the dashed line refers to the intensity at 34 amu. (b) The 10−50 m/z spectrum for a scan at 75 s after initiation of the reaction. Peak assignments (relative intensities) are: $m/z = 14$, N^+ (0.6); $m/z = 16$, O^+ (6.6); $m/z = 17$, $^{16}OH^+$ (8.3); $m/z = 18$, $^{16}OH_2^+$ (35.7); $m/z = 20$, $^{18}OH_2^+$; $m/z = 28$, N_2^+ (26.2); $m/z = 32$, $^{32}O_2^+$ (99.6); $m/z = 34$, $^{34}O_2^+$ (100); $m/z = 36$, $^{36}O_2^+$ (8.0); $m/z = 40$, Ar^+ (0.5); $m/z = 44$, CO_2^+ (1.3).

gas formation was observed within the reaction cell, which was reflected in a large immediate increase in the intensities at 32 and 34 amu, with a much smaller increase occurring at 36 amu. Typically, data were collected for a period of time corresponding to about one turnover of the catalyst, as determined by measuring the rate of O_2 formation with a Clark electrode. For the reaction conditions given in Figure 1, the single turnover time was ∼125 s. The slow decrease observed in the rate of formation of $^{34}O_2$ relative to that of $^{32}O_2$ over the course of the reaction can therefore be attributed to substitution of $H_2{}^{16}O$ at the isotopically labeled *cis*-aqua position during cycling of the catalyst.

Control experiments were performed in which Ce^{4+} was injected into identical solutions that contained no catalyst; in these cases, no increase in intensities as 32, 34, and 36 amu were detected. The mass intensity at 28 amu (corresponding to N_2) also underwent no significant change during the course of injecting oxidant and subsequent O_2 formation in the catalyzed reaction. Barely detectable increases were observed in the mass intensity at 44 amu (corresponding to natural abundance CO_2),

Table 1. Relative Contributions of Pathways Calculated from O_2 Isotopic Distributions[a]

$[Ru_2O]$ (mM)	conditions[b]	$^{32}O_2$[c]	$^{34}O_2$[c]	$^{36}O_2$[c]	class i[d]	class ii[e]	class iii[f]
0.037	28 °C	0.54	0.46	0.006	<0.01	0.49	0.51
0.10	28 °C	0.49	0.49_5	0.015	0.01	0.44	0.55
0.10	28 °C	0.49	0.50	0.008	<0.01	0.45	0.55
0.25	10 °C	0.37	0.62	0.011	<0.01	0.31	0.69
0.27	28 °C	0.40	0.58	0.022	0.01	0.35	0.64
0.29	28 °C	0.50	0.48	0.020	0.05	0.48	0.47
0.29	47 °C	0.59	0.40	0.015	<0.01	0.57	0.43
0.80	28 °C	0.21	0.71	0.080	<0.01	0.15	0.85
0.86	ambient	0.30	0.64	0.058	−0.01	0.32	0.69
0.74	ambient, 92% D_2O	0.36	0.60	0.037	<0.01	0.45	0.55

[a] Calculated as indicated in the Experimental Section. [b] For all reactions, $[Ce^{4+}] = 25$ mM, $[CF_3SO_3H] = 0.5$ M. [c] Fractional yields extrapolated to $t = 0$. [d] Both O atoms from {5,5} terminal ruthenyl (Ru═O) groups. [e] Both O atoms from solvent H_2O. [f] One O atom from Ru═O and one O atom from H_2O.

which appeared to become more pronounced with time of exposure to Ce^{4+}. A representative mass spectrum, taken 75 s following addition of Ce^{4+}, is shown in Figure 1b. Collectively, these results indicate that the observed increase in O_2 mass intensities following oxidant addition arise solely from catalyzed water oxidation, that reagent manipulations introduce no detectable adventitious air, and that oxidative degradation of the catalyst is minimal despite being exposed to a large (30-fold to 250-fold) excess of Ce^{4+} ion.

Another property of the {5,5} ion revealed by these studies is that exchange between the coordinated ruthenyl oxygen and solvent H_2O must be slow relative to catalytic evolution of O_2. Otherwise, one would have observed a rapid change in the relative rates of $^{32}O_2$ and $^{34}O_2$ formation following addition of Ce^{4+} as this process occurred in parallel with water oxidation. In any event, the measured O_2-isotope distributions were corrected for possible minor changes that might have arisen by O-atom exchange, as well as any influence of oxidative modification of the catalyst, by the manner in which the data were analyzed. Specifically, the relative intensities at 32, 34, and 36 amu measured were plotted against time; in the early stages of the reaction, that is, the first 20−40 mass spectral scans, these changes were linear. Extrapolation to $t = 0$, the point at which Ce^{4+} was introduced, gave values for the isotope distributions of O_2 formed at the start of the reaction, a point at which the isotopic distributions in the catalyst and solution were accurately known. The extrapolated values for the various reaction conditions investigated are listed in Table 1.

Solvent Deuterium Isotope Effects. We have previously estimated the kinetics of decay of electrochemically prepared {5,5} ion using both RR and optical spectrometric detection.[7] These methods are experimentally challenging because, in the former case, the {5,5} ion undergoes photoreduction in the relatively intense laser beam used to obtain the RR spectra[7] and, in the latter case, the optical spectra of the {5,5} and {4,4} ions are very similar and decay of the {4,4} ion to {3,4} is sufficiently rapid to interfere with the {5,5} → {4,4} transformation (Scheme 1). In reinvestigating the {5,5} decay kinetics, we have obtained reproducible data by monitoring the relatively small optical changes at the isosbestic points for the {3,4} and {4,4} visible bands, which were at 470 nm in H_2O and 468 nm in D_2O under the prevailing medium conditions. A representative kinetic profile for {5,5} decay is given in Figure 2. The

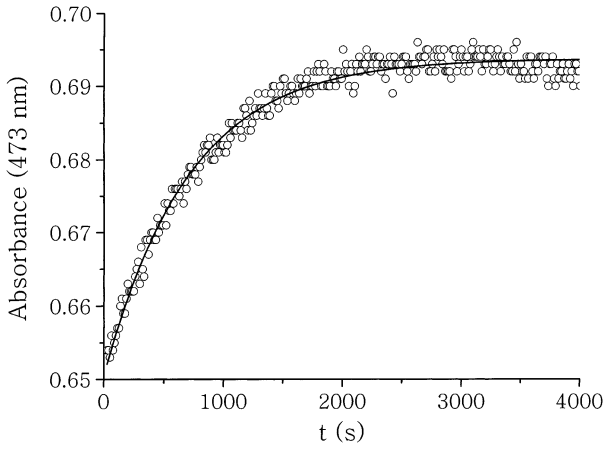

Figure 2. Decay of 0.25 mM electrochemically prepared {5,5} at 13 °C in 0.5 M CF_3SO_3H. The solid line is the exponential fit to the data with $k = 1.42 \times 10^{-3}$ s^{-1}.

measured first-order rate constant in 0.5 M triflic acid at ambient temperature (~23 °C) was $k_{H_2O} = 2.3\ (\pm 0.2) \times 10^{-3}$ s^{-1} and was invariant with reactant concentration over the range [{5,5}] = 0.2−0.7 mM. The rate constant measured in these studies is 4-fold lower than the value we previously reported based upon a more limited data set.[7] The corresponding reaction in 0.5 M triflic acid, 98.9% D_2O, at ambient temperature was $k_{D_2O} = 1.4\ (\pm 0.1) \times 10^{-3}$ s^{-1}, giving a solvent kinetic isotope effect (KIE) of $k_{H_2O}/k_{D_2O} = 1.6$.

As described in the Experimental Section, the rates of O_2 evolution were measured by using a calibrated Clark electrode suspended in the headspace of a closed reaction cell. Reaction was initiated by addition of a 100-fold excess Ce^{4+} to a 0.5 M triflic acid solution containing the {3,3} ion; this amount of Ce^{4+} is sufficient to quantitatively oxidize the complex to its {5,5} oxidation state. Under these conditions, initial rates of O_2 formation are linearly dependent upon the catalyst concentration.[7,9] No O_2 was detected when the catalyst was omitted from the reaction medium. First-order rate constants (k_{cat}) were determined by dividing the measured evolution rates by the amount of catalyst present in solution. In H_2O containing 0.5 M triflic acid, the value obtained at 23 °C was $k_{cat}(H_2O) = 5.2\ (\pm 1.0) \times 10^{-3}$ s^{-1}; the corresponding value in 99.8% D_2O was $k_{cat}(D_2O) = 3.1\ (\pm 0.1) \times 10^{-3}$ s^{-1}, giving an apparent KIE for catalyzed O_2 evolution of 1.7.

The coordinated H_2O molecules in the {3,4} oxidation state of the μ-oxo ion are strongly acidic and undergo sequential one and two-H^+ deprotonations, that is:

$$(bpy)_2Ru(OH_2)\text{-}O\text{-}Ru(OH_2)(bpy)_2^{5+} \underset{+H^+}{\overset{-H^+}{\rightleftharpoons}} (bpy)_2Ru(OH_2)\text{-}O\text{-}Ru(OH)(bpy)_2^{4+} \quad (K_{1a})$$

$$(bpy)_2Ru(OH_2)\text{-}O\text{-}Ru(OH)(bpy)_2^{4+} \underset{+H^+}{\overset{-H^+}{\rightleftharpoons}} (bpy)_2Ru(OH)\text{-}O\text{-}Ru(OH)(bpy)_2^{3+} \quad (K_{2a})$$

with reported ionization constants of $pK_{1a} \simeq 0.4$ and $pK_{2a} \simeq 3.2$ at room temperature.[1] In 99% D_2O, the fully protonated {3,4} ion exhibits a symmetric visible absorption band at 442

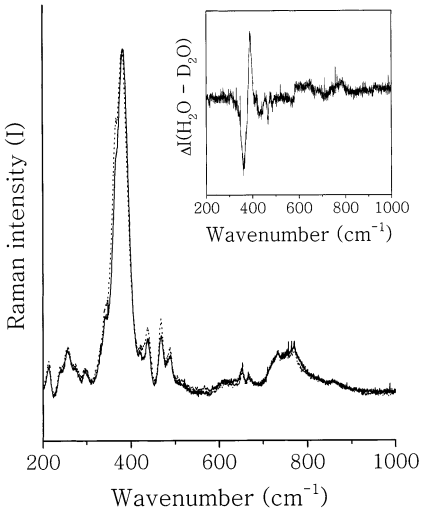

Figure 3. Normalized resonance Raman spectra of 1 mM {3,3} in 0.5 M CF_3SO_3H, H_2O (solid line), and 99.7% D_2O (dashed line). Spectra are the average of 10 scans with 10 s accumulation times at 647 nm. The intense band at ~370 cm^{-1} is attributable to the Ru−O−Ru symmetric stretching mode (ν_s(Ru−O−Ru)).[7] The solvent isotope-dependent shift is evident in the H_2O-D_2O difference spectrum (inset).

nm; a corresponding symmetric band appears at 494 nm in the conjugate base. Spectrophotometric titration with 0.05−3.47 M triflic acid in D_2O gave a value for p$K_{1a}(D_2O) \simeq 0.69$. Thus, the equilibrium isotope ratio for the first ionization constant is $K_{1a}(H_2O)/K_{1a}(D_2O) \simeq 1.9$.

The symmetric stretching frequency (ν_s) of the bridging Ru−O−Ru unit in the {3,3} and {3,4} ions appeared at slightly lower energies ($\Delta\nu = 2-5$ cm^{-1}) in the room-temperature RR spectra of acidic D_2O solutions than in the corresponding spectra in H_2O. Representative spectra are given in Figure 3. These results are very similar to data reported earlier on frozen solutions at 90 K.[13] Confirmation of this effect in the liquid phase is important, however, because the solvent-induced shifts are small and the low temperatures and long acquisition times required to obtain high quality spectra on the instrumentation used in the earlier studies could have introduced artifacts associated with imposition of the solid matrix or photodecomposition in the exciting beam.

Temperature Dependence of O_2 Evolution and {5,5} Decay. The values for k_{cat} increased progressively with temperature from 3.7×10^{-3} s^{-1} to 4.5×10^{-2} s^{-1} over the temperature range of 10−60 °C. A plot of ln(k_{cat}/T) vs T^{-1} (Figure 4) was nearly linear and gave $\Delta H^{\ddagger} = 7.6$ (±1.2) kcal/mol and $\Delta S^{\ddagger} = -43$ (±4) cal/deg mol (23 °C) as apparent activation parameters. Direct optical spectrophotometric measurement of the decay of electrochemically prepared {5,5} to {4,4} over the temperature range of 13−41 °C gave similar values of $\Delta H^{\ddagger} = 7.9$ (±1.1) kcal/mol and $\Delta S^{\ddagger} = -44$ (±4) cal/deg mol (Figure 4).

Discussion

Relative Contributions of the Pathways. The mechanistic model used here to analyze the measured isotopic distributions of O_2 is predicated upon the assumption that exchange does not occur in the μ-oxo bridge during catalytic turnover. We have established this point in previous studies by examining the position of the prominent Ru−O−Ru symmetric stretching mode (ν_s(Ru−O−Ru)) in the RR spectrum of the {3,4} ion.[7,13]

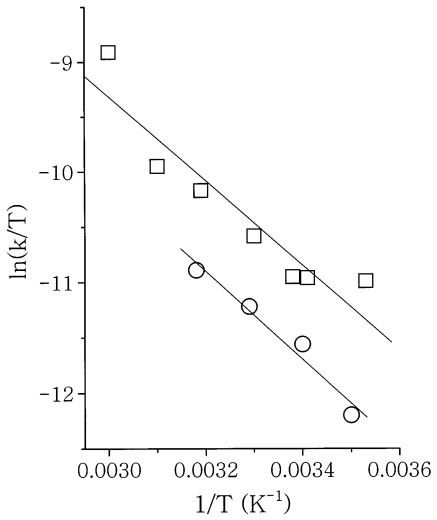

Figure 4. Temperature dependence of first-order rate constants for O_2 evolution (□) and {5,5} decay (○). Conditions: 100 μM {3,3} plus 11 mM Ce^{4+} (O_2 evolution) or 0.25 mM {5,5} (decay) in 0.5 M CF_3SO_3H. Solid lines are linear least-squares fits to the data.

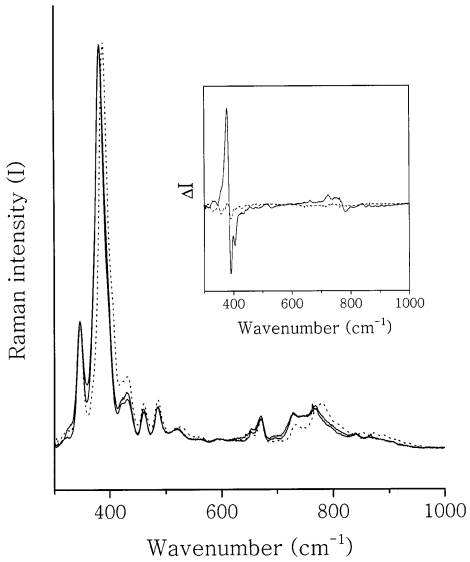

Figure 5. Normalized resonance Raman spectra of 0.18 mM {3,4} in 0.5 M CF_3SO_3H. Spectra are averages of 10 6-s accumulations taken with 40 mW excitation at 488 nm. Solid lines: spectra of {3,4} containing ^{18}O in the μ-oxo bridge before and after complete reaction with 7.2 mM Ce^{4+}; dashed line: spectra of {3,4} containing ^{16}O in the μ-oxo bridge. The intense ^{18}O-isotope dependent band at ~390 cm^{-1} is attributable to (ν_s(Ru−O−Ru)), and the weaker band at ~780 cm^{-1} is attributable to its first overtone ($2\nu_s$(Ru−O−Ru)).[7] The inset shows the $^{18}O-^{16}O$ difference spectrum (solid line) and the difference spectrum obtained for the ^{18}O-substituted ion before and after 10 cycles of the catalyst (dashed line).

As shown in Figure 5, this band appears at 389 cm^{-1} in the solution spectra when the bridge contains ^{16}O and at 382 cm^{-1} when the bridge contains ^{18}O; the large $^{18}O-^{16}O$ difference spectrum provides a sensitive measure of isotopic substitution at that position. However, no difference peaks appear in the spectra of the {3,4} ion recorded before and after >10 catalytic cycles of water oxidation using either Co^{3+} or Ce^{4+} as oxidants (Figure 5).[7,13] This clearly demonstrates the absence of O-substitution within the bridge following repetitive cycling of the catalyst, not only justifying the analytical model but also allowing one to eliminate from consideration pathways such as those shown in Scheme 2, pathway *B*, that involve formation

of symmetric di-μ-oxo bridged intermediates within a single complex ion.[25] Specifically, if this were the mechanism, one would predict substantial substitution within the bridge after only a single turnover. These experiments do not exclude similar di-μ-oxo-bridged intermediates that might be formed by bridging between terminal *cis*-oxo ligands of two complex ions, as recently discussed by Meyer and associates.[12] However, as discussed in the succeeding paragraph, pathways of the latter type are effectively excluded by the isotope distribution patterns observed in these studies.

Listed in Table 1 are the results of calculations that allow one to distinguish between three classes of reaction pathways based upon the molecular origins of O atoms in the O_2 products, namely: (i) both atoms derived from the ruthenyl oxo atoms, (ii) both atoms derived from solvent H_2O, or (iii) one atom from each source. The results of these calculations (Table 1) clearly indicate that contribution of pathways of class i are negligible under all reaction conditions investigated. The small amount of $^{36}O_2$ that is formed is attributable almost entirely to reaction between $[(bpy)_2Ru(^{18}O)]_2O^{4+}$ and $H_2{}^{18}O$ by class iii pathways. Consequently, it can be concluded that **all** unimolecular and bimolecular reactions that involve direct O−O bond formation between *cis*-ruthenyl oxygens are negligible and can be excluded from further consideration. This includes pathways *A*, *B*, and *D* shown in Scheme 2, as well as additional similar pathways discussed by Meyer and co-workers.[12] Furthermore, relative contributions of the other two pathways are large and demonstrably temperature-dependent (Table 1), indicating that solvent is an obligatory participant in O_2 formation that acts by at least two distinct mechanisms.[26] These results are totally consistent with earlier data that we reported for reactions of the same complex ion with Co^{3+} at ambient temperature,[13] but differ from data reported by Geselowitz and Meyer, who found substantially higher relative yields of $^{36}O_2$ in reactions carried out using Ce^{4+} as oxidant.[27] The basis for these differences is uncertain, but the earlier data[13,27] were considerably less accurate because they involved relatively infrequent bolus addition of accumulated gases into the mass spectrometer.

Temperature Dependence and Reaction Models. The existence of at least two reaction pathways is suggested from the temperature dependence of the O_2 isotopic distributions (Table 1). In contrast, Eyring plots for catalyzed rates of O_2 evoluton and {5,5} decay are linear within experimental uncertainty (Figure 4). This temperature dependence is consistent with two simple reaction models, in which either a common intermediate is formed in the rate-limiting step or there are two independent concurrent pathways for reaction between {5,5} and solvent whose activation enthalpies ($\Delta H^{\ddagger}$) are fortuitously similar (Scheme 3). For the former model, the relative yields of isotopic products are governed by the rates of decomposition of the intermediate by the two pathways, but the overall rates

Scheme 3. Kinetic Models for First-Order Decay of the {5,5} Ion

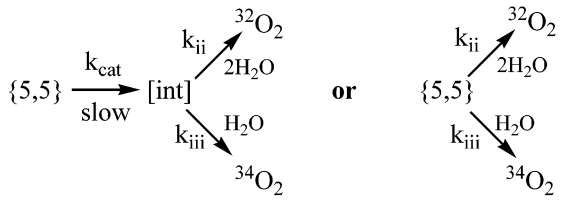

Scheme 4. Hypothetical Intermediates for O−O Bond Formation by the k_{iii} Pathway

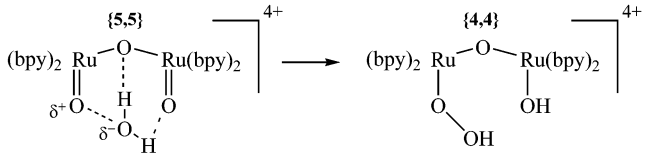

of O_2 formation and {5,5} decay are independent of how the intermediate partitions. For the latter model, the observed temperature dependence of the isotopic yields should also appear in the overall rate of O_2 formation, which is equal to the sum of the decay rates by the various pathways. This model could be excluded if the activation parameters for the two steps predicted significant curvature in the Eyring plots. The differences in activation parameters between reactions forming $^{32}O_2$ and $^{34}O_2$ calculated from the data in Table 1 assuming this model are $\Delta(\Delta H^{\ddagger}) \simeq 5.3$ kcal/mol and $\Delta(\Delta S^{\ddagger}) \simeq 17$ eu. Combining these data with the activation parameters obtained from Figure 4, one calculates values of $\Delta H^{\ddagger} \simeq 10.2$ kcal/mol and $\Delta S^{\ddagger} \simeq -34$ eu for the class ii pathway and $\Delta H^{\ddagger} \simeq 5.0$ kcal/mol and $\Delta S^{\ddagger} \simeq -51$ eu for the class iii pathway. Eyring plots made using these parameters showed the expected curvature, but the magnitude of deviation from linearity was within the uncertainty of the experimental data. Thus, the temperature dependence of rates and relative yields cannot be used in this instance to distinguish between the two reaction models.

Reaction Mechanisms. Class iii Pathway. We have previously suggested that this pathway involves nucleophilic attack of H_2O upon an electrophilic ruthenyl O atom, as illustrated by the structure in Scheme 4. Hydrogen bonding to the adjacent bridging O atom may facilitate O−O bond formation both by properly orienting and increasing the nucleophilicity of the water molecule. The solvent dependence of ν_s(Ru−O−Ru) in the {3,3} and {3,4} ions (Figure 3) provides indirect evidence for this type of interaction. Although the D_2O-induced shifts are small, they are comparable to shifts measured in biological M−O−M centers, for example, the Fe−O−Fe unit in hemerythrin,[28] where H-bonding to the μ-oxo bridge has been confirmed by X-ray crystallography.[29]

Experimental data obtained for oxidation of O−H and C−H bonds in peroxides,[30] hydroquinones,[31] alcohols,[32,33] and arenes[34,35] by monomeric ruthenyl polypyridyl compounds (e.g., $[(bpy)_2(py)Ru^{IV}O]^{2+}$) strongly suggest that these reactions

(25) Mechanisms of this type have been previously suggested within the context of biological water oxidation, based primarily upon the observation that certain di-μ-oxo copper complexes transform reversibly into μ-η^2-η^2-bound O_2 molecule upon changing the solvent composition of the medium (Halfen, J. A.; Mahapatra, S.; Wilkinson, E. C.; Kaderli, S.; Young, V. G., Jr.; Que, L.; Zuberbhhler, A. D.; Tolman, W. B. *Science* **1996**, *271*, 1397−1400).

(26) It is perhaps useful to note that these conclusions were already evident from the raw data; that is, before the analyses described in the Experimental Section were performed. Since the complex was ∼90% enriched in *cis*-$[^{18}O]H_2O$ and the solvent typically contained <3% $[^{18}O]H_2O$, the measured relative yields of $^{36}O_2$, $^{32}O_2$, and $^{34}O_2$ must reflect fairly closely the relative contributions of pathways i−iii, respectively.

(27) Geselowitz, D. A.; Meyer, T. J. *Inorg. Chem.* **1990**, *29*, 3894−3896.

(28) Shiemke, A. D.; Loehr, T. J.; Sanders-Loehr, J. *J. Am. Chem. Soc.* **1986**, *108*, 2437−2443.

(29) Stenkamp, R. E. *Chem. Rev.* **1994**, *94*, 715−726.

(30) Gilbert, J.; Roecker, L.: Meyer, T. J. *Inorg. Chem.* **1987**, *26*, 1126−1132.

(31) Binstead, R. A.; McGuire, M. E.; Dovletoglou, A.; Seok, W. K.; Roecker, L. E.; Meyer, T. J. *J. Am. Chem. Soc.* **1992**, *114*, 173−186.

(32) Thompson, M. S.; Meyer, T. J. *J. Am. Chem. Soc.* **1982**, *104*, 4106−4115.

(33) Roecker, L.; Meyer, T. J. *J. Am. Chem. Soc.* **1987**, *109*, 746−754.

(34) Bryant, J. R.; Mayer, J. M. *J. Am. Chem. Soc.* **2003**, *125*, 10351−10361.

(35) Bryant, J. R.; Matsuo, T.; Mayer, J. M. *Inorg. Chem.* **2004**, *43*, 1587−1592.

proceed by hydride[33] or hydrogen atom abstraction[30,33,34,36] (alternatively, proton-coupled electron transfer[31]) mechanisms. The unusually strong O−H bond in H_2O poses severe energetic constraints on these types of mechanisms for water oxidation by the {5,5} ion. If a similar mechanism is operative, then H-atom abstraction must also be coupled to formation of a peroxo O−O bond because intermediary formation of a discrete hydroxyl radical, even if H-bonded to the μ-oxo atom, is energetically prohibitive.[37] Direct formation of a peroxo-bound {4,4} ion by a concerted mechanism such as that shown in Scheme 4 may also be slightly endergonic. From the relevant two-electron potentials, one calculates $\Delta E^\circ = -0.19$ V for the reaction, $\{5,5\} + 2H_2O \rightarrow \{4,4\} + H_2O_2$; the analogous reaction to form a peroxo anion stabilized by coordination to a highly charged ruthenium center in the {4,4} ion should have similar thermodynamic values. The thermodynamic driving force for the overall reaction, $2\{5,5\} + 2H_2O \rightarrow 2\{4,4\} + O_2$, is large, with $\Delta E^\circ = 0.71$ V; for this mechanism, the overall reaction would therefore be driven to completion by the highly exergonic reaction between the intermediate or H_2O_2 and an additional {5,5} ion.

A more serious mechanistic issue arises from the absence of an appreciable KIE when the reactions were run in D_2O. On basis of the nature of the postulated reaction intermediate, one would expect relatively large KIEs resulting from substantial stretching of the O−H bond in the transition state if the reaction involved rate-limiting bimolecular interaction between H_2O and the {5,5} ion. Indeed, one characteristic feature of the oxidation reactions of the monomeric ruthenyl analogues, for example, $[(bpy)_2(py)Ru^{IV}O]^{2+}$, is their pronounced primary KIEs, which typically exceed values of 20.[30−34] In contrast, the apparent KIE for reaction of the {5,5} ion was only 1.6. This value includes contributions from both class ii and class iii pathways. The very small change in the $^{32}O_2/^{34}O_2$ distribution measured in D_2O under these conditions (Table 1) indicates that the pathways leading to formation of each of these products have similar KIEs. If the reaction between solvent and {5,5} is direct (Scheme 3), it follows from the fact that the overall rate of O_2 formation is the sum of the concurrent pathways that neither pathway can have a large KIE. For this reaction model, one calculates from the data (Table 1) that KIE $\simeq$ 2.0 for the class iii pathway and KIE $\simeq$ 1.1 for the class ii pathway. If the reaction proceeds by rate-limiting formation of a common intermediate, one can conclude from the solvent isotope dependence on the $^{32}O_2/^{34}O_2$ distribution only that the two pathways for O_2 formation have very similar KIEs. The challenge then remains to identify an intermediate whose rate of formation is not solvent isotope-sensitive.

One candidate for a common reactive intermediate is an EPR-detectable species that appears at 80 K as a minor component in both chemically and electrochemically prepared solutions of the {5,5} ion.[6,7] The intensity of this cryogenic signal is proportional to the {5,5} concentration (unpublished observations). Although the signal is as yet unidentified, its spectroscopic features are consistent with those expected for a ligand radical cation,[38] suggesting the possible existence of an intramolecular redox equilibrium of the type:

$$H^+ + \{5,5\} \rightleftarrows [(bpy)(bpy_\pi^{\bullet+})Ru^{IV}(OH)\text{-}O\text{-}Ru^{V}(O)(bpy)_2]^{5+}$$

in which the {5,5} ion is the predominant species. The π-cation radical is presumably stabilized by protonation of the proximal terminal ruthenyl oxygen and by the $-O-Ru^V(O)(bpy)_2$ unit, which, at least in lower oxidation states, appears by several criteria[1,23,39,40] to be strongly σ-donating relative to simple monomeric $(bpy)_2RuX_2$ analogues and might thereby significantly lower the HOMO of coordinated bipyridine. The "push−pull" asymmetry generated by electronic redistribution within this complex could enhance reactivity by strengthening the H-bond between the μ-oxo atom and the reacting solvent molecule (Scheme 4), thereby increasing its nucleophilicity without proportionately decreasing the electrophilicity of an adjacent Ru^V terminal oxo atom. Additionally, the higher reduction potential of the relatively unstable {4,5}-bipyridyl π-cation radical could be crucial in lowering the thermodynamic barrier to forming a peroxide-bound {4,4} intermediate.

Class ii Pathway. The existence of a pathway by which O_2 is formed catalytically by two solvent molecules was already evident from earlier ^{18}O-labeling experiments.[13,27] Devising a plausible mechanism to account for this reaction, however, has been challenging. This task is not diminished by the recognition from this (Figure 1) and other recent studies[23] that the catalyst does not undergo aqua ligand exchange with solvent during catalysis. We had previously suggested[13] that reactive intermediates with hydroperoxide anions bound to each of the Ru atoms might form, for example, by addition of a second H_2O molecule to the covalent hydrate in Scheme 4 to give a {3,3}-dihydroperoxy complex, as in, for example:

$$[(bpy)_2Ru(OOH)ORu(OH)(bpy)_2]^{4+} + H_2O \rightarrow [(bpy)_2Ru(OOH)]_2O^{2+} + 2H^+ \quad (1)$$

Subsequent intramolecular rearrangement to yield O_2 or H_2O_2 might proceed via a bridging tetroxide intermediate. Meyer has suggested[14] a similar possibility involving a bridging ozonide dianion (O_3^{2-}) that could conceivably also be formed by rearrangement of the covalent hydrate shown in Scheme 4 (e.g., by analogy to the formation of hydrogen trioxide (H_2O_3) from the combination of perhydroxyl ($HO_2^\bullet$) and hydroxyl ($OH^\bullet$)).[41−43] Subsequent attack by solvent at the central O atom could then give O_2 in which both O atoms are obtained from solvent.[14]

These intermediates are plausible in the sense that H_2O_3 is a well-established chemical entity[44−47] and that experimental

(36) Mayer, J. M. *Acc. Chem. Res*. **1998**, *31*, 441−450.
(37) A lower limit on the one-electron potential for {5,5} reduction can be estimated from the measured $\{5,5\} \rightarrow \{4,4\}$ potential (E° {5,5}/{4,4} = 1.59 V) and the apparent lack of {4,5} formation during redox titrations of the μ-oxo ion.[7] Assuming that accumulation of {4,5} is less than 10% of the total dimer concentration, the comproportionation constant (K_c) for the reaction, $\{5,5\} + \{4,4\} \rightleftharpoons 2\{4,5\}$ is $K_c \lesssim 10^{-2}$, from which one calculates E° {5,5}/{4,5} $\lesssim$ 1.5 V. Using $E^\circ(OH^\bullet/OH^-) = 2.02$ V (*CRC Handbook of Chemistry and Physics*, 83rd ed.; Lide, D. R., Ed.; CRC Press: Boca Raton, FL, 2002−2003), it follows that $\Delta E^\circ \lesssim -1.3$ V for the reaction $\{5,5\} + H_2O \rightarrow \{4,5\} + OH^\bullet$.
(38) See, for example: (a) DeArmond, M. K.; Hanck, K. W.; Wertz, D. W. *Coord. Chem. Rev.* **1985**, *64*, 65−81. (b) Kaim, W. *Coord. Chem. Rev.* **1987**, *76*, 187−235.
(39) Dobson, J. C.; Sullivan, B. P.; Doppelt, P.; Meyer, T. J. *Inorg. Chem*. **1988**, *27*, 3863−3866.
(40) Doppelt, P.; Meyer, T. J. *Inorg. Chem*. **1987**, *26*, 2027−2034.
(41) Czapski, G.; Bielski, B. H. J. *J. Phys. Chem*. **1963**, *67*, 2180−2184.
(42) Bielski, B. H. J.; Schwarz, H. A. *J. Phys. Chem*. **1968**, *72*, 3836−3841.
(43) Bielski, B. H. J. *J. Phys. Chem*. **1968**, *72*, 3836−3841.
(44) Deglise, X.; Giguère, P. A. *Can. J. Chem*. **1971**, *49*, 2242−2247.
(45) Cerkovnik, J.; Plesničar, B. *J. Am. Chem. Soc*. **1993**, *115*, 12169−12170.

evidence also exists for the formation of hydrogen tetroxide (H_2O_4);[44] the hypothetical oxo-polyoxo dibridged intermediates represent ruthenium-coordinated analogues of the hydrogen polyoxides. Both polyoxides are unstable; unimolecular decomposition of H_2O_3 gives O_2 ($^1\Delta$) as a product, and oxidized water species are also produced upon decomposition of the less well-characterized H_2O_4. Examination of structural models suggests that there are no large steric restrictions to formation of mixed dibridged complexes of the catalyst containing the analogous dianions. However, reactions involving formation of either intermediate may be untenable on energetic grounds.[7] Specifically, the reaction $\{4,4\} + H_2O_2 + H_2O \rightarrow \{3,3\} + H_2O_3$ can be used as a rough guide for the energetics of the reaction $[(bpy)_2Ru(OOH)ORu(OH)(bpy)_2]^{4+} \rightarrow [((bpy)_2Ru_2)(\mu\text{-}O)(\mu\text{-}1,3\text{-}O_3)]^{2+} + 2H^+$; on the basis of a recent estimate for the enthalpy of formation for H_2O_3 of $\Delta H_f^\circ = -23$ kcal/mol,[48] with the assumption that entropy contributions approximately cancel, one calculates $\Delta E^\circ \sim -0.7$ V for the former reaction. Similarly, one obtains $\Delta E^\circ \sim -0.5$ V as an estimate of the energetics of reaction 1 using previously determined redox potentials[7] for the reaction $\{4,4\} + 2H_2O \rightarrow \{3,3\} + H_2O_2$. Formation of both dibridged intermediates should be considerably less favorable than these estimates because in both cases they require release of protons to the highly acidic medium and are accompanied by reduction of the overall electrostatic charge on the complex from 4+ to 2+, thereby decreasing coordinate bond stabilization. Consistent with this view, recent ab initio calculations suggest that pathways for unimolecular decomposition of H_2O_3 involve either acid catalysis or participation of solvent as a bifunctional catalyst in concerted proton donor−acceptor reactions;[46,49−51] in these studies, no low energy pathways involving nucleophilic attack of the O atom of a water molecule on the central O atom of H_2O_3 have been identified. If analogous mechanisms are applied to decomposition of the hypothetical $[((bpy)_2Ru)_2(\mu\text{-}O)(\mu\text{-}1,3\text{-}O_3)]^{2+}$ intermediate, $^{34}O_2$, rather than $^{32}O_2$, would be the isotopic product of the ^{18}O-labeled ruthenium complexes. Thus, these putative low energy pathways cannot account for the appearance of $^{32}O_2$ in the product gases (Figure 1). The activation barrier for reaction 1 must also be relatively high because the reactant ruthenium complex contains no ruthenyl group to initiate H-atom abstraction from H_2O.

Formation of O_2 from two H_2O's might involve expansion of a Ru(V) coordination sphere by addition of H_2O, which then undergoes subsequent reaction with a second solvent molecule. Some support for this notion is obtained from the kinetics of water exchange on monomeric Ru(III) centers, which suggest that an associative interchange mechanism is operative,[52] and discussions that encompass a wider chemical literature of seven-coordinate species.[53] However, if this mechanism were operative, one might expect that the intermediate would also provide a pathway for facile exchange of the *cis*-ruthenyl oxygen atoms in {5,5} with solvent H_2O, which is not observed. Furthermore, it is difficult to rationalize by this type of mechanism why monomeric analogues of the type, *cis*-$L_2Ru(OH_2)_2^{2+}$, and dinuclear ions not containing the $(H_2O)RuORu(OH_2)$ core, for example, $[(bpy)_2(py)RuORu(H_2O)(bpy)_2]^{4+}$, appear incapable of catalyzing water oxidation.[40,54]

"Spontaneous" oxidation of $Ru(bpy)_3^{3+}$ and similar strongly oxidizing group 8 polypyridyl complexes in alkaline solutions has been reported by several groups.[15−18] In general, these reactions involve predominantly oxidation of the bipyridine ligands, accompanied by copious evolution of CO_2 and the appearance of numerous ruthenium(II)-containing products bearing modified ligands. However, Ledney and Dutta have reported that, when the $Ru(bpy)_3^{3+}$ ions are entrapped within zeolite cages, complex decomposition is minimal and water oxidation becomes particularly efficient.[18] These researchers have argued that this occlusion of the catalyst effectively blocks the bimolecular ligand decomposition pathways which dominate the chemistry in homogeneous solution, allowing expression of the water oxidation pathway. For the same reason, these reactions apparently do not require formation of the μ-oxo dimer (or other multinuclear complex ion intermediates) that have been proposed to be the actual catalysts of OH^- oxidation by $Ru(bpy)_3^{3+}$.[55] The mechanism proposed by Ledney and Dutta for this reaction[18] involves initial nucleophilic addition of OH^- to an electrophilic carbon atom on one of the bipyridine rings, forming a relatively stable ligand-centered radical complex of Ru(II). Subsequent one-electron oxidation of the metal center yields a Ru(III)−ligand radical species that is primed for reaction with a second OH^- to give H_2O_2 and $Ru(bpy)_3^{2+}$ as final products. Support for this reaction model includes the kinetics of $Ru(bpy)_3^{2+}$ formation, which are first-order in $[Ru(bpy)_3^{3+}]$ and $[OH^-]$ under most reaction conditions in homogeneous solution,[15] as well as demonstrations that $Ru(bpy)_3^{3+}$ and similar M(III) group 8 complexes readily undergo analogous nucleophilic addition reactions to give ring-modified polypyridine ligands,[19,21] among which is apparent addition of H_2O to give covalent hydrates,[22] and that reaction between radiolytically generated $OH^\bullet$ and $Ru(bpy)_3^{3+}$ or various $M(bpy)_3^{2+}$ ions gave products with spectroscopic signatures[15] that are very similar to optically detectable intermediates appearing in the $Ru(bpy)_3^{3+}$−OH^- reaction.

A bipyridine ligand-based mechanism for class ii water oxidation by {5,5} that incorporates key features of the $Ru(bpy)_3^{3+}$ reactions is given in Scheme 5. The reaction is initiated by addition of the elements of water to form a covalent hydrate in which OH^- is added to a bipyridine ligand and H^+ protonates a terminal ruthenyl O atom. This reaction would also be considerably facilitated by internal electronic rearrangement that generated a {4,5}-$bpy^{\bullet+}$ radical cation. Alternatively, covalent hydrate formation might be promoted by H-atom abstraction at a Ru═O center in a concerted reaction similar to that proposed for the class iii reaction (Scheme 4). In this case, the OH segment is positioned to add to the ring six-position to form a {4,5} intermediate containing a neutral ligand radical (Scheme 5). In this manner, the reaction could avoid intermediary formation of the {4,5}-$bpy^{\bullet+}$ radical cation. The neutral radical also represents an alternative candidate for the cryogenic EPR signal detected in frozen solutions of the {5,5} ion.[6,7,18]

(46) Plesničar, B.; Tuttle, T.; Cerkovnik, J.; Koller, J.; Cremer, D. *J. Am. Chem. Soc.* **2003**, *125*, 11553−11564.
(47) Engdahl, E.; Nelander, B. *Science* **2002**, *295*, 482−483.
(48) Lay, T. H.; Bozzelli, J. W. *J. Phys. Chem. A* **1997**, *101*, 9505−9510.
(49) Koller, J.; Plesničar, B. *J. Am. Chem. Soc.* **1996**, *118*, 2470−2472.
(50) Mckay, D. J.; Wright, J. S. *J. Am. Chem. Soc.* **1998**, *120*, 1003−1013.
(51) Xu, X.; Muller, R. P.; Goddard, W. A., III. *Proc. Natl. Acad. Sci. U.S.A.* **2002**, *99*, 3376−3381.
(52) Rappaport, I.; Helm, L.; Merbach, A. E.; Bernhard, P.; Lundi, A. *Inorg. Chem.* **1988**, *27*, 873−879.
(53) Serpone, N.; Ponterini, G.; Jamieson, M. A.; Bolletta, F.; Maestra, M. *Coord. Chem. Rev.* **1983**, *50*, 209−302.
(54) Collin, J. P.; Sauvage, J. P. *Inorg. Chem.* **1986**, *25*, 135−141.
(55) Lay, P. A.; Sasse, W. H. F. *Inorg. Chem.* **1985**, *24*, 4707−4710.

Scheme 5. Hypothetical Intermediates for O−O Bond Formation by the k_{ii} Pathway

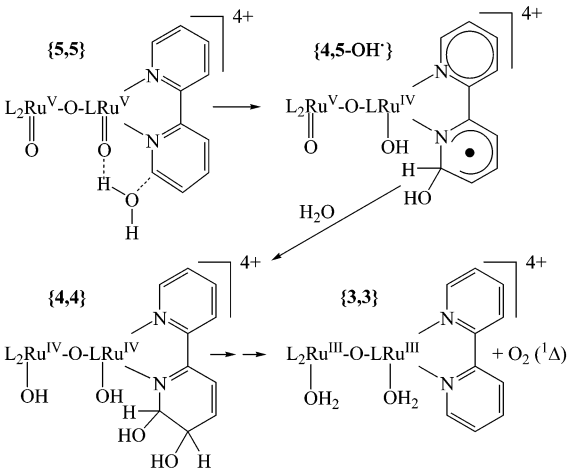

Specifically, internal ligand-to-metal electron transfer could be fairly slow, as has been demonstrated for the $[(NH_3)_5Copy-OH^{\bullet}]^{3+}$ radical adduct,[56] allowing accumulation of the ligand radical to EPR-detectable levels during catalyst turnover. Subsequent addition of a second H_2O molecule to the modified bipyridine ring to form a {4,4}-coordinated bipyridine diol (Scheme 5) is suggested by analogy to similar reactions proposed in the overall reactions between $Ru(bpy)_3^{3+}$ and OH^- that lead to ligand decomposition.[17] This reaction would be facilitated in the dinuclear μ-oxo ion by the pendant $[(bpy)_2Ru(=O)O]^+$ moiety, which can function as an electron sink for the unpaired electron. Unlike monomeric $Ru^{II}(bpy)_2(bpy(OH)_2)^{2+}$ analogues, the bipyridine diol in the dinuclear ion is coordinated to a two-electron oxidizing center which is nearly as strongly oxidizing as the original {5,5} ion. Additional internal electron transfer could drive oxidation of the OH substituents to form, for example, an unstable endoperoxide[57] that undergoes further bond rearrangement to give O_2 and the {3,3} ion. In this context, one should note that identification of the actual site(s) of OH attachment to the ring is not intended in Scheme 5. Addition at other sites might well occur and could significantly affect catalysis. For example, addition at the heterocyclic N or bridging C positions would be expected to minimize competing pathways leading to oxidative degradation of the ligand.

Additional Comments. The mechanism presented here is a minimal scheme that best accommodates the existing data and is subject to refinement as detectable intermediates become better characterized. For example, the rate constants for first-order decay of {5,5} measured by optical spectroscopy vary by as much as 4-fold under different experimental conditions (cf., our reported values at 23 °C in this work and ref 7), which might ultimately be attributable to the appearance of strongly absorbing intermediates. Furthermore, the mass spectral kinetic profiles obtained immediately following addition of Ce^{4+} suggest that there is a very short induction period prior to formation of $^{32}O_2$ that is not observed for $^{34}O_2$. This behavior is consistent with accumulation of a reactive intermediate in the class ii pathway that is not required for the class iii pathway, a circumstance that would require expansion of the simple mechanisms given in Scheme 4. Similarly, the increase in $^{34}O_2/^{32}O_2$ ratio observed at the highest {5,5} concentrations (Table 1, data for 28 °C) might be indicative of minor contribution from a bimolecular pathway involving, for instance, reaction between an intermediate species and {5,5}. Identification of the anomalous signal in the low-temperature EPR spectra of the complexes, currently in progress, is expected to elucidate many of these mechanistic issues.

Acknowledgment. We thank Joseph T. Hupp (Northwestern University) and Carl C. Wamser (Portland State University) for helpful discussions and Pierre Moënne-Loccoz (OGI School of Science & Engineering, Oregon Health & Science University, Portland, OR) for technical assistance in acquiring the resonance Raman spectra. This work is supported financially by the Division of Chemical Sciences, Office of Basic Energy Sciences, U.S. Department of Energy, under Grant DE-FG03-99ER14943.

JA030594G

(56) Hoffman, M. Z.; Kimmel, D. W.; Simic, M. G. *Inorg. Chem*. **1979**, *18*, 2479−2485.
(57) Wasserman, H. H.; Scheffer, J. R. *J. Am. Chem. Soc*. **1967**, *89*, 3073−3075.